Microsyst Technol (2011) 17:1747–1754
DOI 10.1007/s00542-011-1361-4

TECHNICAL PAPER

A scrape-through piezoelectric MEMS energy harvester with frequency broadband and up-conversion behaviors

Huicong Liu · Cho Jui Tay · Chenggen Quan · Takeshi Kobayashi · Chengkuo Lee

Received: 4 August 2011 / Accepted: 28 September 2011 / Published online: 14 October 2011

Abstract We propose a MEMS piezoelectric energy harvester with a wide operating frequency range by incorporating a high-frequency piezoelectric cantilever and a metal base as the top and bottom stoppers with a low-frequency piezoelectric cantilever. Frequency up-conversion of the piezoelectric energy harvester is realized when the low-frequency piezoelectric cantilever impacts and scrapes through the high-frequency piezoelectric cantilever. For an input acceleration of 0.6 g, with top and bottom stopper distances of 0.75 and 1.1 mm, respectively, the operating frequency ranges from 33 to 43 Hz. The output voltage and power up to 95 mV and 94 nW can be achieved. Experimental results indicate that the frequency up-conversion mechanism significantly improves the effective power.

1 Introduction

MEMS-based energy harvesting from ambient vibrations provides a clean and regenerative solution for powering autonomous sensors which have been widely utilized in medical, military and general industrial applications (Roundy et al. 2003a; Paradiso and Starner 2005; Mitcheson et al. 2008; Romero et al. 2009). In recent years, a large number of researches on energy harvesting have been done based on piezoelectric (Cook-Chennault et al. 2008; Park et al. 2010; Saadon and Sidek 2011; Liu et al. 2011), electromagnetic (Wacharasindhu and Kwon 2008; Yang et al. 2009, 2010a, 2010b), electrostatic (Lo and Tai 2008; Sakane et al. 2008; Paracha et al. 2009; Yang et al. 2010b) and thermoelectric (Xie et al. 2009, 2010) mechanisms. Conventional vibration-based energy harvesters are developed as a linear resonant system subjected to harmonic vibrations. The major disadvantage is that they have a narrow operating bandwidth which limits their applications in actual environments with random and irregular frequency spectra, since the maximum power generation occurs only when the environmental vibration falls within the bandwidth at or near the resonant frequency (Williams and Yates 1996).

To overcome such limitation, many attempts have been made to increase the operating frequency range by tuning or widening the resonant frequency (Zhu et al. 2010). Several approaches have been reported in frequency tunable energy harvesters by varying the length of a piezoelectric cantilever (Gieras et al. 2007), applying axial compressive load to a piezoelectric bimorph (Leland and Wright 2006), and varying the spring stiffness of a cantilever by using magnetic force (Erturk et al. 2009; Stanton et al. 2009). However, these approaches require additional systems or energy in order to tune the center frequency. Integration of an array of generators with different mechanical resonant frequencies provides a wide operating bandwidth (Shahruz 2006; Sari et al. 2008). However, this approach would result in an increase in the

H. Liu · C. J. Tay · C. Quan
Department of Mechanical Engineering, National University of Singapore, 9 Engineering Drive 1, Singapore 117576, Singapore

T. Kobayashi
National Institute of Advanced Industrial Science and Technology (AIST), 1-2-1 Namiki, Tsukuba, Ibaraki 305-8564, Japan

C. Lee (✉)
Department of Electrical and Computer Engineering, National University of Singapore, 4 Engineering Drive 3, Singapore 117576, Singapore
e-mail: elelc@nus.edu.sg

size of the device. By using a mechanical stopper, a wideband energy harvester is reported (Liu et al. 2011). A wideband micro electrostatic energy harvester is realized by using nonlinear springs (Nguyen et al. 2010), although this design requires an additional bias voltage. A bi-stable mechanism has been reported as a potential method for broadening the bandwidth (Jung and Yun 2010), while a wideband operation frequency is realized by using electrostatic levitation and nonlinear springs (Suzuki et al. 2010).

According to the studies (Roundy et al. 2003b, Miller et al. 2011), most common environmental vibrations are in the low frequency range (<200 Hz). To generate sufficient output power for low frequency applications, frequency up-conversion technologies have been reported by several researchers. A piezoelectric membrane is used to generate energy due to impact caused by a steel ball (Umeda et al. 1996). Besides, it has also reported a non-resonant energy harvester driven by a periodical impact of a free moving ball between two piezoelectric benders (Renaud et al. 2009). It has been reported that a novel frequency up-conversion (FUC) approach by releasing a piezoelectric bimorph and achieving self-oscillation based on the mechanical cyclic-contact between the probe of a piezoelectric bimorph and the superelastic ridges attached onto a micro slider mechanism (Lee et al. 2007). An impact-driven piezoelectric energy harvesting device is demonstrated by using an ABS beam sandwiched with two PZT bimorphs (Gu and Livermore 2011). This mechanism utilizes a low-frequency resonator to impact a high-frequency resonator in order to trigger a self-oscillation and generate power at high frequency. It is reported that magnetic force is deployed to mediate the interaction between a low-frequency driving diaphragm and a high-frequency generating cantilever. A magnet periodically catches and releases a magnetic strip mounted on the cantilever, resulting in a high-frequency self-oscillation of the cantilever and hence increasing the energy harvesting efficiency (Kulah and Najafi 2008). A microfabricated version of this device was also reported later (Sari et al. 2010). An innovative frequency up-conversion method uses a diaphragm with a magnet to collect energy a vibration shaker. The vibrating diaphragm would scrape through the tip of a cantilever which is fixed to a supporting base. Electrical current is subsequently generated through the winding coil on the cantilever (Zorlu et al. 2011).

In this work, we have investigated energy harvesting from the aspects of widening the operating frequency range and frequency up-conversion. The unique impact mechanism including scrape-through and release between the two piezoelectric cantilevers is presented. The device configuration based on a scrape-through approach and its fabrication and operating mechanism are also described. A model providing the theoretical power is included as well.

2 Device configuration and operating mechanism

A schematic diagram of the proposed scrape-through piezoelectric energy harvester is shown in Fig. 1a. It comprises of a low-frequency piezoelectric PZT cantilever (termed as PZT-L cantilever) and a high-frequency piezoelectric PZT cantilever (termed as PZT-H cantilever) assembled with a pre-determined gap. The dimensions of the PZT cantilevers are shown in Table 1. The PZT-L cantilever consists of a beam attached with a silicon proof mass for harvesting energy from ambient low-frequency vibrations. Along the longitudinal direction of the beam, PZT thin film patterns are deposited and parallel arrayed. The top and bottom electrodes of each PZT thin film pattern are connected to their individual bonding pads on the base of the PZT-L cantilever. Likewise, the PZT-H cantilever has the same beam as the PZT-L cantilever but without additional proof mass in order to achieve high natural frequency. The resonant frequencies of the PZT-L and PZT-H cantilevers are 36 and 618 Hz, respectively. As shown in Fig. 1b, the PZT-H cantilever which acts as a top-stopper is mounted at a vertical distance of d_1 above the proof mass of the PZT-L cantilever and in the horizontal direction it overlaps the proof mass by a length of l. The bottom surface of the proof mass is at a distance d_2 from the metal base which acts as a bottom-stopper.

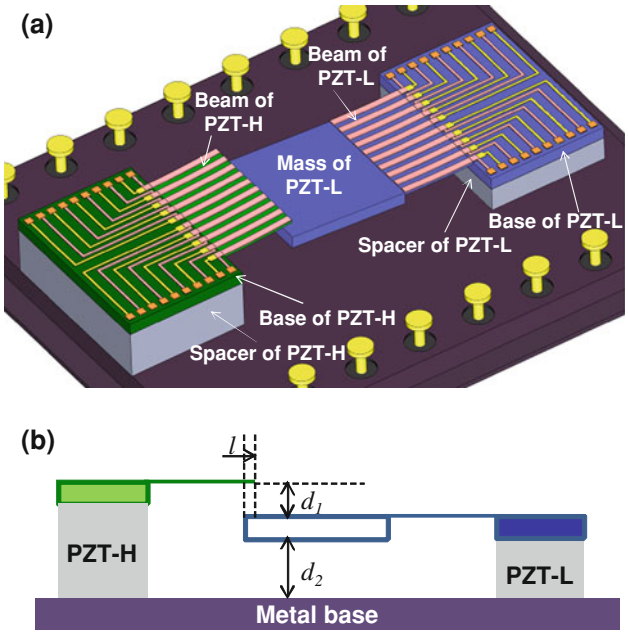

Fig. 1 Schematic diagram of a scrape-through piezoelectric energy harvester

Table 1 Structural parameters and material properties of the piezoelectric PZT cantilevers

	Parameter	Value
Structural parameters	Length of cantilever beam	3 mm
	Width of cantilever beam	5 mm
	Thickness of cantilever beam	5 μm
	Length of proof mass	5 mm
	Width of proof mass	5 mm
	Thickness of proof mass	0.4 mm
	Length of PZT pattern	3 mm
	Width of PZT pattern	0.24 mm
	Thickness of PZT pattern	3 μm
Material properties	Young's modulus of PZT	72 GPa
	Relative dielectric constant of PZT	1,000
	Piezoelectric constant of PZT	−50 pm/V
	Young's modulus of Silicon	190 GPa

Figure 2 illustrates the operating mechanism of the proposed scrape-through piezoelectric energy harvester. When the vibration amplitude of the PZT-L cantilever is sufficiently large, the proof mass will periodically impact the PZT-H cantilever and metal base. As a result, the operating bandwidth of the PZT-L cantilever will be broadened, at the expense of retardation in the vibration amplitude. Detailed analytical and numerical descriptions of the frequency wideband response can be found in (Narimani et al. 2004; Soliman et al. 2008, 2009). The overlapping length l is adjusted such that the proof mass of the PZT-L cantilever is able to scrape through the tip of the PZT-H cantilever during impact. Considering a particular instant of an oscillation cycle when the proof mass is at its lowest point at position① (Fig. 2a) and starts to move to position② where the proof mass starts to impact the beam of the PZT-H cantilever. At this instant, the proof mass and the beam would move upward in tandem. During this movement, the overlapping distance between the proof mass and the beam decreases continuously until it reaches a critical position③ when the beam would scrape through the proof mass and is released to self-oscillate at its own resonant frequency. Thereafter the proof mass continues its upward movement until it reaches its maximum amplitude at position③*. Then it would start to move downward until another critical position④, where the overlapping distance between the proof mass and the beam is again reduced to zero. From position④, the proof mass scrapes through again to position④* and the beam is again released to self-oscillate while the proof mass moves back to position①. The cycle is repeated as the proof mass moves toward position② again. During each vibration cycle, the mass of the PZT-L cantilever impacts, scrapes through and releases the beam of the PZT-H cantilever twice, resulting in the PZT-H cantilever oscillating at its high resonant frequency of 618 Hz. The cyclic deformation of the PZT layer on the beams of the PZT-L and PZT-H cantilevers would result in an electrical output due to piezoelectric effect.

3 Modeling and microfabrication

For a vibration-based beam with a mass attached at its tip, the strain distribution on the beam top surface $\xi_{1L}(x)$ can be derived by assuming a concentrated force applied at the middle of the mass and is given by (Beer and Johnston 1992; Roundy 2003; Kamal et al. 2010),

$$\xi_{1L}(x) = \frac{3t_b}{l_b}\left(\frac{2l_b + l_m - 2x}{4l_b^2 + 9l_b l_m + 6l_m^2}\right)\delta_m \quad (1)$$

Likewise, the strain distribution on the top surface $\xi_{1H}(x)$ of a beam without the mass is derived by considering a concentrated force applied at the beam tip and is given by

$$\xi_{1T}(x) = \frac{3t_b(l_b - x)}{2l_b^3}\delta_b \quad (2)$$

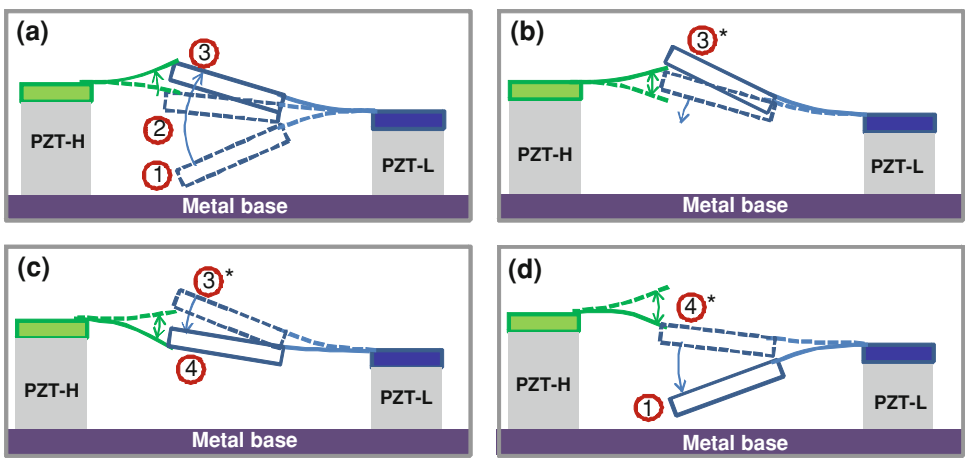

Fig. 2 Operating mechanism of the proposed scrape-through piezoelectric energy harvester

where δ_m is the mass tip deflection for a beam with a mass attached, δ_b is the beam tip deflection for a beam without a mass, l_m is the proof mass length, l_b and t_b are the beam length and thickness, respectively, x refers to the variable distance between the beam fixed end and its tip. The generated open circuit voltage of a beam with deposition of piezoelectric layer would depend on the properties of the piezoelectric material and the strain distribution along the piezoelectric layer as

$$V_{o.c.} = \frac{-d_{31} Y t_e}{\varepsilon_{33} l_b} \int_0^{l_b} \xi_1(x) dx \tag{3}$$

where Y is the Young's modulus of the piezoelectric material, d_{31} is the transverse-axial piezoelectric constant, ε_{33} is the transverse dielectric coefficient, t_e is the thickness of the piezoelectric layer. Hence, the open circuit voltages of the PZT-L and PZT-H cantilevers are expressed as

$$V_{o.c.L} = \frac{-d_{31} Y t_e}{\varepsilon_{33} l_b} \frac{3(l_b + l_m) t_b \delta_m}{4l_b^2 + 9 l_b l_m + 6 l_m^2} \tag{4}$$

$$V_{o.c.H} = \frac{-d_{31} Y t_e}{\varepsilon_{33}} \frac{3 t_b \delta_b}{4 l_b^2} \tag{5}$$

The generated electrical power delivered to the connected load can therefore be written as

$$P_{rms} = \frac{1}{2} \frac{V_{o.c.}^2}{(Z_P + Z_L)^2} Z_L \tag{6}$$

where Z_P is the piezoelectric impedance and Z_L is the load impedance. The maximum power transfer occurs when the load impedance Z_L matches with the piezoelectric impedance Z_P.

Figure 3 shows the fabrication process of a MEMS piezoelectric PZT cantilever. A SOI wafer with a 5 μm Si device layer, a 1 μm buried oxide layer and a 400 μm Si handle layer was used in the fabrication. As shown in Fig. 3a, the SOI wafer was first oxidized at 1,100°C to form a thermal oxide layer. This was followed by deposition of a Pt/Ti layer by DC magnetron sputtering as a bottom electrode layer. A 3-μm-thick (100)-oriented PZT layer was then formed by sol–gel deposition (Kobayashi et al. 2005). It was followed by deposition of a Ti/Pt/Ti layer as a top electrode layer. In Fig. 3b, the top electrode layer was patterned by Ar-ion beam etching, followed by wet-etching of the PZT layer using a mixture of HF, HNO_3 and HCl. The same process was applied to the patterning of the bottom electrode layer. A SiO_2 layer of 1-μm-thick which acts as an insulation layer as shown in Fig. 3c was then deposited by RF-magnetron sputtering. As shown in Fig. 3d, contact holes were then etched on the isolation layer by reactive ion etching (RIE) using CHF_3 gas, followed by deposition and patterning of Pt metal lines and bonding pads. To release the beam, RIE from the front side was carried out with gases of CHF_3 and SF_6 as shown in Fig. 3e. A final deep RIE process was applied from the back side to etch the Si handle layer and buried oxide layer until the proof mass was released completely, as shown in Fig. 3f.

4 Results and discussion

The fabricated piezoelectric PZT cantilevers are shown in Fig. 4a (PZT-H cantilever) and Fig. 4b (PZT-L cantilever). An enlarged section of the highlighted area is show in

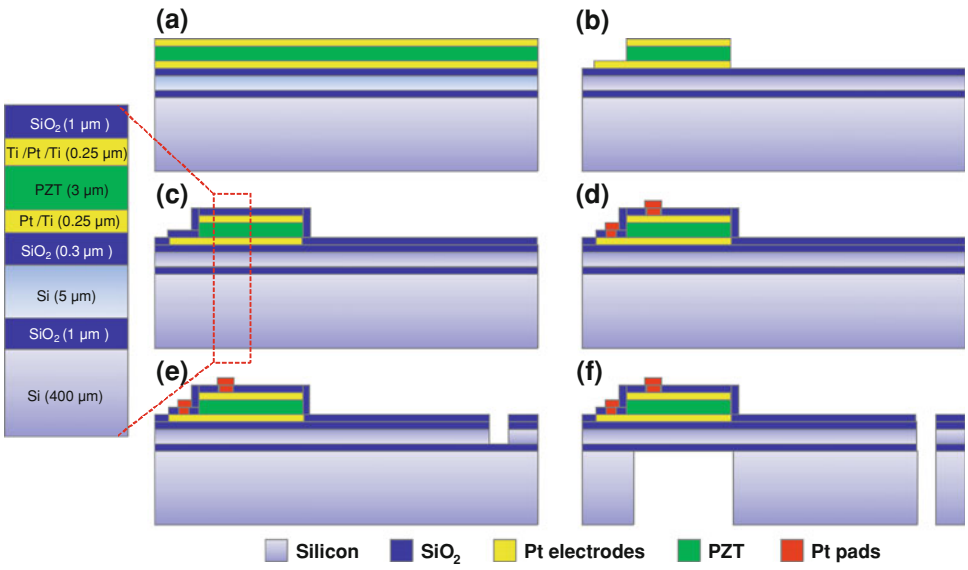

Fig. 3 Microfabrication process of the piezoelectric PZT cantilever

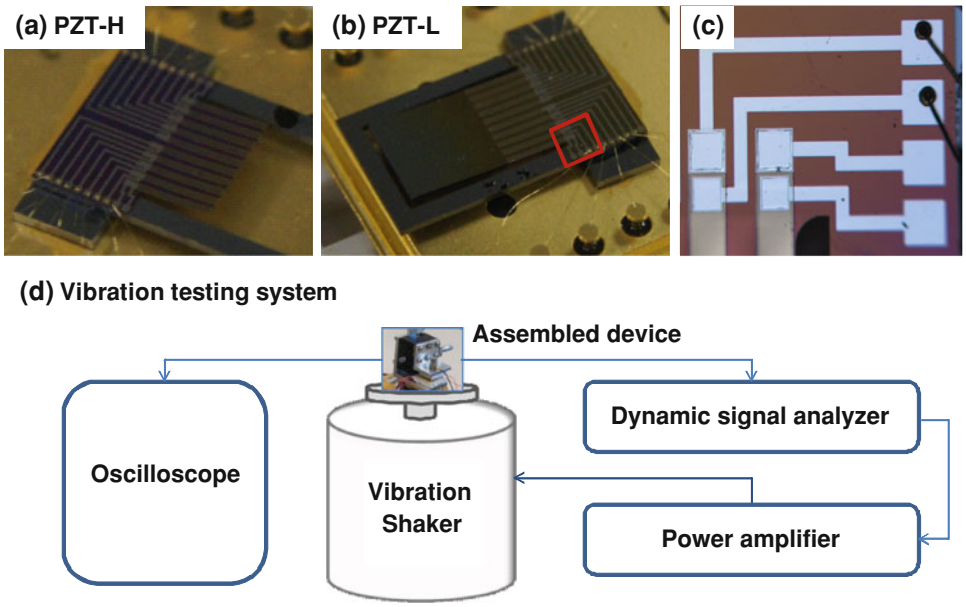

Fig. 4 Microfabricated piezoelectric PZT cantilever devices of (**a**) PZT-H cantilever and (**b**) PZT-L cantilever; **c** Enlarged view of the highlighted (*red*) area in Fig. 4b; **d** Experimental setup of the vibration testing system

Fig. 4c. The assembled energy harvester device is characterized by using the vibration testing system as shown in Fig. 4d. It consists of an electromagnetic vibration shaker, a power amplifier, a dynamic signal analyzer and an oscilloscope. The vibration frequency and amplitude of the shaker are controlled by a dynamic signal analyzer through an amplifier. The output voltages of both the PZT-L and PZT-H cantilevers are recorded via the dynamic signal analyzer and an oscilloscope.

The output rms voltages of the PZT-L cantilever against the sweeping frequency from 20 to 60 Hz for a top-stopper distance of 0.75 mm and a bottom-stopper distance of 1.1 mm and input accelerations of 0.1–0.6 g are shown in Fig. 5. It is seen that at a relatively low input acceleration of 0.1 g, a maximum output rms voltage of 62 mV is generated at a relatively low resonant frequency of 36 Hz. At an input acceleration of 0.2 g, the PZT-L cantilever engages the PZT-H cantilever which acts as a top stopper and the operating frequency bandwidth is increased (34.5–37.5 Hz) with a corresponding increase in the output rms voltage (70–81 mV). When the input acceleration is increased to 0.6 g, the operating frequency bandwidth is further increased from 33 to 43 Hz, while the output rms voltage is increased from 76 to 95 mV.

Figure 6a shows the instantaneous output voltages of the PZT-L and PZT-H cantilevers at excitation frequency of 36 Hz and input acceleration of 0.6 g. Fig. 6b shows an enlarged view of the dotted box shown in Fig. 6a. It is seen in Fig. 6b that the average peak-to-peak voltage of the PZT-L cantilever is around 0.23 V. During each vibration cycle, the PZT-L cantilever impacts, scrapes through and releases the PZT-H cantilever twice, resulting in a self-oscillation of the PZT-H cantilever at its high resonant frequency of 618 Hz. Due to mechanical damping effect, the voltage generated by the PZT-H cantilever is exponentially attenuated and the average peak-to-peak voltage is 0.11 V. The beam tip displacement of the PZT-H cantilever and the mass tip displacement of the PZT-L cantilever are calculated using Eqs. 4 and 5 and are shown in Fig. 7a. Figure 7b is an enlarged view of the tip displacements of the dotted box as shown in Fig. 7a. The critical positions in one oscillation cycle of the PZT-H cantilever as demonstrated in Fig. 2 are also indicated. At position②, the PZT-L cantilever impacts the PZT-H cantilever and moves upward together to position③, where the mass of the PZT-L cantilever just scrapes through the beam of the PZT-H cantilever, and thus the PZT-H cantilever is released to self-oscillate at its resonant frequency. At

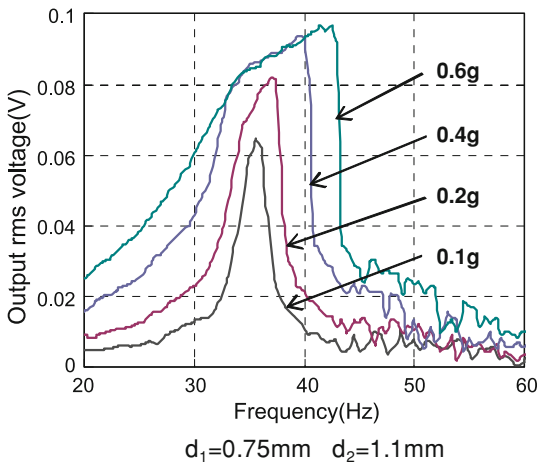

Fig. 5 Voltage rms output against frequencies for different input accelerations

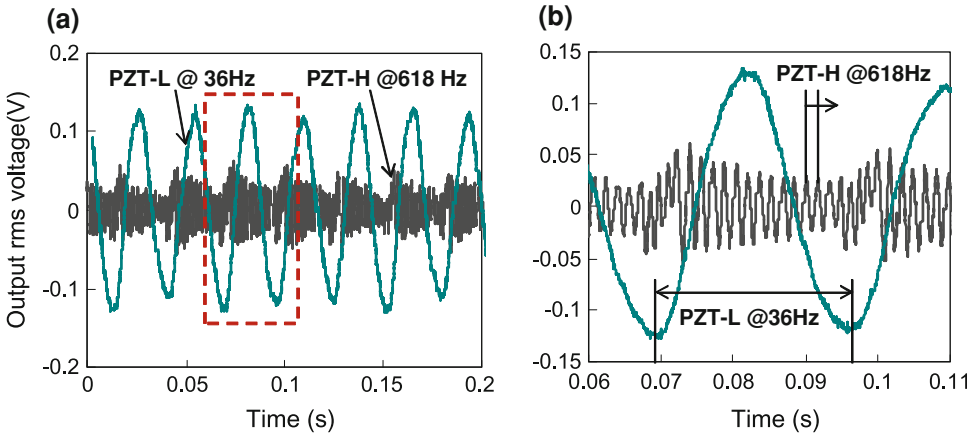

Fig. 6 **a** Instantaneous output voltages of the PZT-L and PZT-H cantilevers at excitation frequency of 36 Hz and input acceleration of 0.6 g; **b** Enlarged view of the highlighted (*red dotted box*) voltage output wave

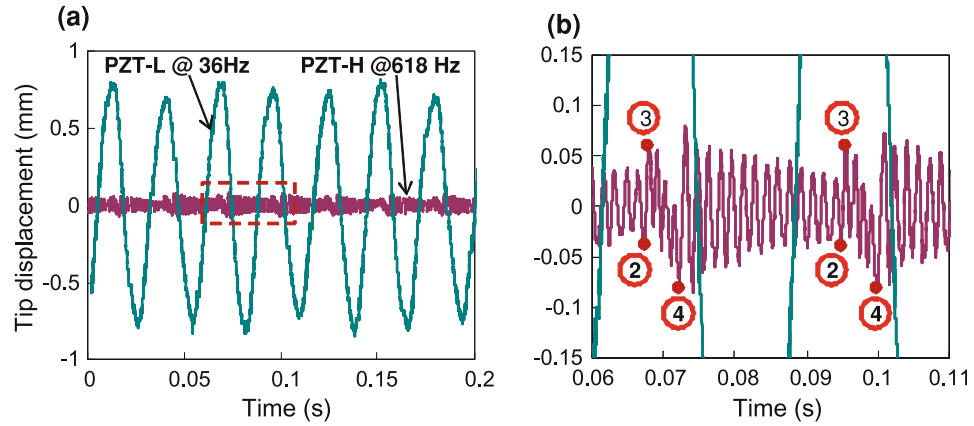

Fig. 7 **a** Instantaneous tip displacements of the PZT-L and PZT-H cantilevers at excitation frequency of 36 Hz and input acceleration of 0.6 g; **b** Enlarged view of the highlighted (*red dotted box*) tip displacement wave

another critical position④, the proof mass scrapes through on the downward movement and the PZT-H cantilever is again left to self-oscillate. The average peak of the tip displacements of the PZT-L and PZT-H cantilevers are around 0.81 and 0.06 mm, respectively.

The optimal power outputs of the PZT-L and PZT-H cantilevers are calculated by using Eq. 6. Figure 8 shows the optimal power outputs against frequencies for input acceleration of 0.1–0.6 g, respectively. For an input acceleration of 0.6 g, the output power varies from 61 to 94 nW within a wideband range of 33–43 Hz. Figure 9a shows the optimal power at an excitation frequency of 36 Hz at 0.6 g over a time period of 0.2 s as shown in Fig. 6. The average peak power of the PZT-L and PZT-H cantilevers are around 145 and 30 nW, respectively. The results indicate that the PZT-H cantilever has a lower output than the PZT-L cantilever. This is mainly due to the much smaller displacement of the PZT-H cantilever and the energy loss during scrape-through process. However, it is observed that effective power of the PZT-H cantilever defined as the mean of output power divided by the average tip displacement (500 nW/mm) is higher than that of the PZT-L cantilever (179 nW/mm). Hence, the PZT-H cantilever would generate a considerably higher power output than the PZT-L cantilever for a given tip displacement. This indicates that the frequency up-conversion mechanism would improve the effective power significantly. The power efficiency of the up-conversion mechanism would also be increased by increasing the effective mass of the PZT-H cantilever and reducing the spring stiffness and

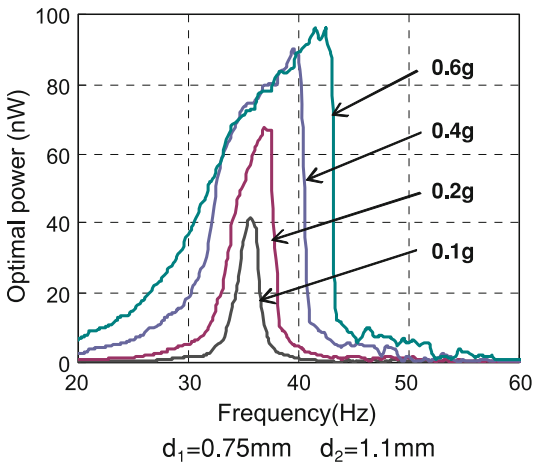

Fig. 8 Optimal power outputs against frequencies under different input accelerations

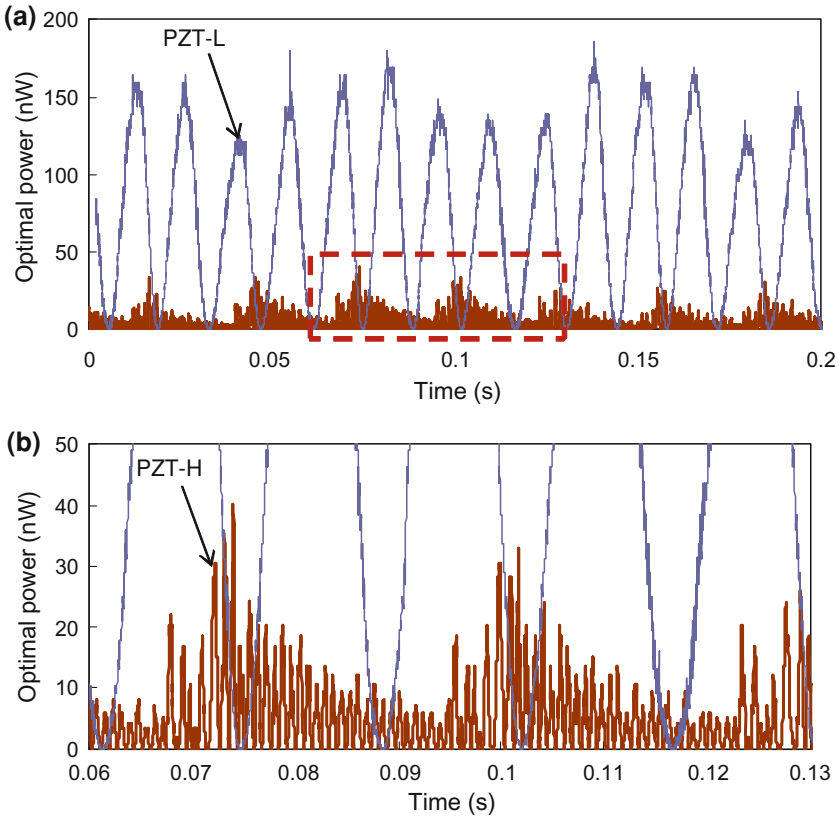

Fig. 9 **a** Instantaneous optimal power of the PZT-L and PZT-H cantilevers at excitation frequency of 36 Hz and input acceleration of 0.6 g; **b** Enlarged view of the highlighted (*red dotted box*) optimal power wave

damping of the PZT-H cantilever. This would increase the tip displacement and subsequently result in a higher output power.

5 Concluding remarks

This paper demonstrates the design, fabrication and measurement of a MEMS-based piezoelectric energy harvester with frequency broadband and up-conversion behaviors. The frequency broadband behavior of the output voltage and power for a PZT-L cantilever is realized by utilizing a PZT-H cantilever and a metal base as mechanical stoppers. The frequency up-conversion behavior of the PZT-H cantilever is achieved by a scrape-though process driven by ambient low-frequency vibrations. It is noteworthy that the proposed scrape-through energy harvester has a major advantage of utilizing both frequency broadband and up-conversion mechanisms simultaneously. With proper and optimized stopper distance, we can realize the chip-scale-packaged MEMS-based piezoelectric energy harvester by using low temperature solder-based bonding technology (Yu et al. 2009; Lee et al. 2009). Thus, ultracompact piezoelectric energy harvester can be fabricated in such a way. Besides, this mechanism shows a good potential as a power source in wireless microsystems operating at low-frequency and irregular vibrations.

Acknowledgments This work was partially supported by in research grant of MOE Tier-2 Academic Research Committee (ARC) Fund MOE2009-T2-2-011 (R-263000598112) at the National University of Singapore.

References

Beer FP, Johnston ER (1992) Mechanics of materials. McGraw-Hill Inc, New York

Cook-Chennault KA, Thambi N, Sastry AM (2008) Powering MEMS portable devices: a review of non-regenerative and regenerative power supply systems with special emphasis on piezoelectric energy harvesting systems. Smart Mater Struct 17:043001

Erturk A, Hoffmann J, Inman DJ (2009) A piezomagnetoelastic structure for broadband vibration energy harvesting. Appl Phys Lett 94:254102

Gieras JF, Oh J-H, Huzmezan M, Sane HS (2007) Electromechanical energy harvesting system. US Patent Application Publication US 2009/0079200 A1

Gu L, Livermore C (2011) Impact-driven, frequency up-converting coupled vibration energy harvesting device for low frequency operation. Smart Mater Struct 20:045004

Jung SM, Yun KS (2010) Energy-harvesting device with mechanical frequency-up conversion mechanism for increased power efficiency and wideband operation. Appl Phys Lett 96:111906

Kamal TM, Elfrink R, Renaud M, Hohlfeld D, Goedbloed M, De Nooijer C, Jambunathan M, Van Schaijk R (2010) Modeling and characterization of MEMS-based piezoelectric harvesting devices. J Micromech Microeng 20:105023

Kobayashi T, Ichiki M, Tsaur J, Maeda R (2005) Effect of multi-coating process on the orientation and microstructure of lead

zirconate titanate (PZT) thin films derived by chemical solution deposition. Thin Solid Films 489:74–78
Kulah H, Najafi K (2008) Energy scavenging from low-frequency vibrations by using frequency up-conversion for wireless sensors applications. IEEE Sens J 8:261–268
Lee DG, Carman G-P, Murphy D, Schulenburg C (2007) Novel micro vibration energy harvesting device using frequency up conversion. Proceedings of 14th international conference on solid-state sensors, actuators and microsystems (IEEE transducer 07), pp 871–874
Lee C, Yu A, Yan L, Wang H, He JH, Zhang QX, Lau JH (2009) Characterization of intermediate In/Ag layers of low temperature fluxless solder based wafer bonding for MEMS packaging. Sens Actuators A 154(1):85–91
Leland E, Wright P (2006) Resonance tuning of the piezoelectric vibration energy scavenging generators using compressive axial preload. Smart Mater Struct 15:1413–1420
Liu H, Tay CJ, Quan C, Kobayashi T, Lee C (2011) Piezoelectric MEMS energy harvester for low frequency vibrations with wideband operation range and steadily increased output power. IEEE J Microelectromech Syst 20(5):1131–1142
Lo H, Tai Y (2008) Parylene-based electrets power generators. J Micromech Microeng 18:104006
Miller LM, Halvorsen E, Dong T, Wright PK (2011) Modeling and experimental verification of low-frequency MEMS energy harvesting from ambient vibrations. J Micromech Microeng 21:045029
Mitcheson PD, Yeatman EM, Rao GK, Holmes AS, Green TC (2008) Energy harvesting from human and machine motion for wireless electronic devices. Proc IEEE 96:1457–1486
Narimani A, Golnaraghi MF, Jazar GN (2004) Frequency response of a piecewise linear vibration isolator. J Vib Control 10:1775–1794
Nguyen DS, Halvorsen E, Jensen GU, Vogl A (2010) Fabrication and characterization of a wideband MEMS energy harvester utilizing nonlinear springs. J Micromech Microeng 20:125009
Paracha AM, Basset P, Galayko D, Marty F, Bourouina T (2009) A silicon MEMS DC/DC converter for autonomous vibration-to-electrical-energy scavenger IEEE electron. Device Lett 30(5):481–483
Paradiso JA, Starner T (2005) Energy scavenging for mobile and wireless electronics. IEEE Pervasive Comput 4:18–27
Park JC, Park JY, Lee YP (2010) Modeling and characterization of piezoelectric d33-mode MEMS energy harvester. J Microelectromech Syst 19:1215–1222
Renaud M, Fiorini P, van Schaijk R, van Hoof C (2009) Harvesting energy from the motion of human limb: the design and analysis of an impact-based piezoelectric generator. Smart Mater Struct 18:035001
Romero E, Warrington RO, Neuman MR (2009) Energy scavenging sources for biomedical sensors. Physiol Meas 30:R35–R62
Roundy SJ (2003) Energy scavenging for wireless sensor nodes with a focus on vibration to electricity conversion. PhD thesis, University of California
Roundy S, Wirght PK, Rabaey JM (2003a) Energy scavenging for wireless sensor networks, 1st edn. Kluwer Academic, Boston
Roundy S, Wright PK, Rabaey J (2003b) A study of low level vibrations as a power source for wireless sensor nodes. Comput Commun 26:1131–1144
Saadon S, Sidek O (2011) A review of vibration-based MEMS piezoelectric energy harvesters. Energy Convers Manage 52:500–504
Sakane Y, Suzuki Y, Kasagi N (2008) Development of high-performance perfuluoriented polymer electret film and its application to micro power generation. J Micromech Microeng 18:104011
Sari I, Balkan T, Kulah H (2008) An electromagnetic micro power generator for wideband environmental vibrations. Sensors Actuators A 123–124:63–72
Sari I, Balkan T, Kulah H (2010) An electromagnetic micro power generator for low-frequency environmental vibrations based on the frequency upconversion technique *J*. Microelectromech Syst 19:14–27
Shahruz SM (2006) Design of mechanical band-pass filters for energy scavenging. J Sound Vib 292:987
Soliman MSM, Abdel-Rahman EM, El-Saadany EF, Mansour RR (2008) A wideband vibration-based energy harvester. J Micromech Microeng 18:115021
Soliman MSM, Abdel-Rahman EM, El-Saadany EF, Mansour RR (2009) A design procedure for wideband micropower generators. J Microelectromech Syst 18:1288–1299
Stanton SC, McGehee CC, Mann BP (2009) Reversible hysteresis for broadband magnetopiezoelastic energy harvesting. Appl Phys Lett 95:174103
Suzuki Y, Miki D, Edamoto M, Honzumi M (2010) A MEMS electret generator with electrostatic levitation for vibration-driven energy-harvesting applications. J Micromech Microeng 20:104002
Umeda M, Nakamura K, Ueha S (1996) Analysis of transformation of mechanical impact energy to electrical energy using a piezoelectric vibrator *Japan*. J Appl Phys 35:3267–3273
Wacharasindhu T, Kwon JW (2008) A micromachined energy harvester from a keyboard using combined electromagnetic and piezoelectric conversion. J Micromech Microeng 18:104016
Williams CB, Yates RB (1996) Analysis of a micro-electric generator for microsystems. Sens. Actuators A: Phys 52:8–11
Xie J, Lee C, Wang MF, Liu Y, Feng H (2009) Characterization of heavily doped polysilicon films for CMOS-MEMS thermoelectric power generators. J Micromech Microeng 19:125029
Xie J, Lee C, Feng H (2010) Design, fabrication and characterization of CMOS MEMS-based thermoelectric power generators. IEEE J Microelectromechanical Syst 19(2):317–324
Yang B, Lee C (2010) Non-resonant electromagnetic wideband energy harvesting mechanism for low frequency vibrations. Microsyst Technol 16(6):961–966
Yang B, Lee C, Xiang W, Xie J, He JH, Kotlanka RK, Low SP, Feng H (2009) Electromagnetic energy harvesting from vibrations of multiple frequencies. J Micromech Microeng 19:035001
Yang B, Lee C, Kee WL, Lim SP (2010a) Hybrid energy harvester based on piezoelectric and electromagnetic mechanisms. SPIE J of Micro/Nanolithography, MEMS, and MOEMS (JM3) 9(2):023002
Yang B, Lee C, Kotlanka RK, Xie J, Low SP (2010b) A MEMS rotary comb mechanism for harvesting kinetic energy of planar vibrations. J Micromech Microeng 20:065017
Yu D-Q, Lee C, Yan LL, Choi WK, Yu A, Lau JH (2009) The role of Ni buffer layer on high yield low temperature hermetic wafer bonding using In/Sn/Cu metallization. Applied Physics Lett 94:034105
Zhu D, Tudor MJ, Beeby SP (2010) Strategies for increasing the operating frequency range of vibration energy harvesters: a review. Meas Sci Technol 21:022001
Zorlu O, Topal ET, Kulah H (2011) A Vibration-based electromagnetic energy harvester using mechanical frequency up-conversion method. IEEE Sensors J 11:481–488